

Magneto-resistivity model and ionization energy approximation for ferromagnets

Andrew Das Arul Samy,^{1,2,*} Xiangyuan Cui,¹ Catherine Stampfli,¹ and Kurunathan Ratnavelu²

¹*School of Physics, The University of Sydney, Sydney, New South Wales 2006, Australia*

²*Institute of Mathematical Sciences, University of Malaya, 50603 Kuala-Lumpur, Malaysia*

(Dated: February 16, 2019)

The evolution of resistivity versus temperature ($\rho(T)$) curve for different doping elements, and in the presence of various defects and clustering are explained for both diluted magnetic semiconductors (DMS) and manganites. Here, we provide unambiguous evidence that the concept of ionization energy (E_I), which is explicitly associated with the atomic energy levels, can be related quantitatively to transport measurements. The proposed ionization energy model is used to understand how the valence states of ions affect the evolution of $\rho(T)$ curves for different doping elements. We also explain how the $\rho(T)$ curves evolve in the presence of, and in the absence of defects and clustering. The model also complements the results obtained from first-principles calculations.

PACS numbers: 75.70.-i; 71.30.+h; 72.15.Rn; 75.50.Pp

Keywords: Ferromagnets, Valence state, Ionization energy, Resistivity versus temperature curves

I. INTRODUCTION

Spintronics is a field that aims to add spin-dependent functionality into existing charge transport devices [1]. DMS (Ref. 2) have tremendous potential for spintronics-device development, whereas manganites that show a large drop of resistance below T_C lead to the colossal magnetoresistance effect (CMR), which is also important in the new technologies such as read/write heads for high-capacity magnetic storage and spintronics [3]. As such, applications involving both DMS and manganites very much depend on our understanding of their transport properties at various doping levels and temperatures (T). There are several models developed to characterize the resistivity of DMS. In particular, the impurity band model coupled with the multiple exchange interactions for $T < T_C$ for $\text{Ga}_{1-x}\text{Mn}_x\text{As}$ was proposed [4]. The electronic states of the impurity band can be either localized or delocalized, depending on doping concentration or the Fermi-level (E_F). If E_F is in the localized-state, then the conduction is due to carrier hopping. If E_F is in the extended-state, then the conduction is metallic and finite even for $T = 0$ (Ref. 4). On the other hand, the spin disorder scattering resistivity as a function of magnetic susceptibility can be used to estimate the magnitude of J_{ex} (the ferromagnetic (FM) exchange interaction energy) [5]. Moreover, there are also theories that qualitatively explain the conductivity for $T > 0$, namely, the Kohn-Luttinger kinetic exchange model [6] and the semiclassical Boltzmann model [7, 8, 9]. Apart from that, for manganites, the one- and two-orbital models [10] and the phase separated resistivity model [11] have been used to qualitatively describe the resistivity curves for $T > 0$. However, in all these approaches, we are faced with two crucial problems, the need (i) to explain how the resistivity evolve with different doping elements, without any *a priori* assumption on carrier density and (ii) to understand how defects and clustering affect the evolution of $\rho(T)$ curves. Here, we show unequivocally, a new method to analyse the evolution of $\rho(T)$ curves for different doping elements using the concept of the E_I invoked in the Hamiltonian and Fermi-Dirac statistics. In doing so, we can also understand the evolution of $\rho(T)$ curves in the presence of defects and clustering, which is important for characterization of spintronics devices. The E_I concept has broad applications, where it has been applied successfully for the normal state (above critical temperature) of high temperature superconductors [12, 13, 14] and ferroelectrics [15]. The E_I model is for compounds obtained via substitutional doping, not necessarily homogeneous or defect-free.

II. IONIZATION ENERGY MODEL

A. Carrier density

A typical solid contains 10^{23} strongly interacting particles. Therefore, their universal collective behavior is of paramount interest as compared to the microscopic details of each particular particle and the potential that surrounds

*Electronic address: andrew@physics.usyd.edu.au

it. This universal collective behavior, being the focal point in this work, arises out of Anderson's arguments in *More is Different*. [16] That is, we intend to justify a universal physical parameter that could be used to describe the association between the transport-measurement data and the fundamental properties of an atom. In view of this, we report here the existence of such a parameter through the Hamiltonian as given below (Eq. (1)). The parameter is the ionization energy, a macroscopic, many-electron atomic parameter.

$$\hat{H}\varphi = (E_0 \pm \xi)\varphi, \quad (1)$$

where \hat{H} is the usual Hamilton operator and E_0 is the total energy at $T = 0$. The $+$ sign of $\pm \xi$ is for the electron ($0 \rightarrow +\infty$) while the $-$ sign is for the hole ($-\infty \rightarrow 0$). Here, we define the ionization energy in a crystal, $\xi = E_I^{\text{real}}$ is approximately proportional to E_I of an isolated atom or ion. Now, to prove the validity of Eq. (1) is quite easy because ξ is also an eigenvalue and we did not touch the Hamilton operator. Hence, we are not required to solve Eq. (1) in order to prove its validity. We can prove by means of constructive (existence) and/or direct proofs, by choosing a particular form of wavefunction with known solution (harmonic oscillator, Dirac-delta and Coulomb potentials) and then calculate the total energy by comparison. In doing so, we will find that the total energy is always given by $E_0 \pm \xi$, as it should be (see Appendix and Ref. [17]). For an isolated atom, the concept of ionization energy implies that (from Eq. (1))

$$\pm \xi = E_{\text{kin}} - E_0 + V_{\text{pot}} = \pm E_I,$$

where E_I is the ionization energy of an isolated atom. The corresponding total energy is $E_0 \pm \xi = E_{\text{kin}} + V_{\text{pot}} = E_0 \pm E_I$. Whereas for an atom in a crystal, the same concept of ionization energy implies that $\pm \xi = E_{\text{kin}} - E_0 + V_{\text{pot}} + V_{\text{many-body}} = E_I + V_{\text{many-body}} = \pm E_I^{\text{real}}$. Here, V_{pot} is the atomic Coulomb potential, while the $V_{\text{many-body}}$ is the many body potential averaged from the periodic potential of the lattice. The corresponding total energy is $E_0 \pm \xi = E_{\text{kin}} + V_{\text{pot}} + V_{\text{many-body}} = E_0 \pm E_I + V_{\text{many-body}} = E_0 \pm E_I^{\text{real}}$. Here, E_I^{real} is the ionization energy of an atom in a crystal. The exact values of E_I are known for an isolated atom. We also define here, $\beta = 1 + \frac{\langle V(x) \rangle}{E_I}$, where $\langle V(x) \rangle$ is the averaged many-body potential value. That is, one can still use E_I obtained from isolated atoms for $r \rightarrow \infty$ in order to predict the evolution of resistivity versus temperature curves for different doping elements. Therefore, Eq. (1) can be approximately rewritten as $\hat{H}\varphi \propto (E_0 \pm E_I)\varphi$. It is obvious from the Hamiltonian given in Eq. (1) that we cannot use it to determine interactions responsible for FM and the magnitude of T_C , simply because we have suppressed the $V_{\text{many-body}}$. On the other hand, if we have a free-electron system, then the total energy equation is given by $E = E_0 \pm \sum_i^z \sum_j E_{Ii,j}^{\text{real}} = E_0 \pm \beta \sum_j E_{Ij}$, where, E_0 is the total energy of the compound at $T = 0$ and j is the sum over the constituent elements in a particular compound. We have defined, $\beta = 1 + \frac{\langle V(x) \rangle}{E_I}$, where $\langle V(x) \rangle$ is the averaged many-body potential value. The E_I^{real} can be noted as one of the many-body response functions with respect to transport properties. The total energy can be rewritten as

$$\begin{aligned} E &= E_0 \pm \sum_i^z \sum_j E_{Ii,j}^{\text{real}} \\ &= E_0 \pm [E_{\text{kin}} - E_0 + V_{\text{pot}} + V_{\text{many-body}}] \\ &= E_{\text{kin}} + V_{\text{pot}} + V_{\text{many-body}} \Leftrightarrow \text{for electrons } \pm \rightarrow + \\ &= E_{\text{kin}} + V_{\text{total}} \\ &= E_{\text{kin}} \Leftrightarrow \text{implies free electrons.} \end{aligned} \quad (2)$$

Note that we have substituted for E_I^{real} since the concept of ionization energy is irrelevant here simply because the electrons in these metals are free and do not require excitations from its parent atom to conduct electricity. As such, the carrier density is constant and independent of temperature. Whereas, the scattering rate is the one that determines the resistivity with respect to temperature, impurities, defects, electron-electron and electron-phonon interactions. Therefore, the total energy from Eq. (1) carries the *fingerprint* of each constituent atom in a compound and it refers to the difference in the energy levels of each atom rather than the absolute values of each energy level in each atom. Hence, the kinetic energy of each electron from each atom will be captured by the total energy and preserves the atomic level *electronic-fingerprint* in the compound. Parallel to Eq. (1), the electron and hole distribution functions can be derived as [12, 13]

$$f_e(E_0, E_I) = \frac{1}{e^{[(E_0 + E_I) - E_F^{(0)}]/k_B T} + 1},$$

$$f_h(E_0, E_I) = \frac{1}{e^{[E_F^{(0)} - (E_0 - E_I)]/k_B T} + 1}. \quad (3)$$

where $E_F^{(0)}$ is the Fermi level at $T = 0$, independent of doping concentration and k_B is the Boltzmann constant. From Eq. (3), one can surmise that large E_I corresponds to the difficulty of the electron to conduct due to a large Coulomb attraction between the electron and the ionic core. This effect will give rise to low conductivity. The variation of E_I with doping in our model somewhat resembles the variation produced from the impurity band model with doping [4, 18]. The difference is that our model fixes the Fermi level as a constant and we let E_I capture all the changes due to doping, consistent with ionization energy based Fermi-Dirac statistics (iFDS). Whereas, in the impurity-band approach, both the impurity band and the Fermi level evolve simultaneously with doping, consistent with Fermi-Dirac statistics. The carrier density can be calculated from

$$n = \int_0^\infty f_e(E_0, E_I) N_e(E_0) dE_0, \quad (4)$$

where $N_e(E_0)$ is the density of states and E_F is defined from now on as the Fermi level at $T = 0$ so as to comply with Eq. (1).

B. Spin-orbit coupling

Here, we will show the relationship of the ionization energy to the energy level splitting and the spin-orbit coupling, as well as their association with resistivity. It is well established that the energy associated with both the relativistic correction and the spin-orbit coupling for Hydrogen-like atoms is given by the fine structure formula, E_{fs} (Ref. 19)

$$E_{fs} = -\frac{E_n}{n^2} \left[1 + \frac{(\alpha_{fs} Z)^2}{n} \left(\frac{1}{k} - \frac{3}{4n} \right) \right], \quad (5)$$

where α_{fs} is the fine structure constant, $k = j + 1/2$, $j = l \pm 1/2$, where j is the total angular momentum, l is the orbital angular momentum and E_n is the non-relativistic energy level. Z and n are the atomic and the principal quantum numbers, respectively. Using Eqs. (1) and (5), we can show the extreme magnitude of the energy level splitting (i.e., between $k = 1$ and $k = n$) is

$$\Delta E_{fs} = (\alpha_{fs} Z)^2 (E_0 \pm \xi)_n \frac{(n-1)}{n^2}. \quad (6)$$

Thus, the magnitude of the energy level splitting (ΔE_{fs}) is proportional to the ionization energy (ξ) and Z^2 , while it is inversely proportional to n . That is, ΔE_{fs} also decreases with decreasing ionization energy (see Fig. 1). Therefore, we can surmise that a system with large ionization energy gives rise to large spin-orbit coupling, which is important for spin-injection [20] in p -type DMS. As discussed earlier however, a large ionization energy also leads to a small carrier density (from Eq. (4)), which in turn implies that spin-orbit coupling competes with the electrical conductivity. In addition, Fig. 1 points out that $\Delta E_{fs1 \rightarrow 2}$ and $\xi_{1 \rightarrow 2}$ are larger than $\Delta E_{fs1 \rightarrow 3}$ and $\xi_{2 \rightarrow 3}$, respectively, in accordance with Eqs. (5) and (6). Therefore, we can surmise that $\Delta E_{fs1 \rightarrow 2} \propto \xi_{1 \rightarrow 2}$, $\Delta E_{fs1 \rightarrow 3} \propto \xi_{2 \rightarrow 3}$, $\Delta E_{fs1 \rightarrow 4} \propto \xi_{3 \rightarrow 4}$ and so on.

C. Resistivity model based on ionization energy

In order to derive the resistivity model as a function of ionization energy, we need an expression that connects the carrier density with the total current. As a consequence, we propose that the total current in ferromagnets consists of contributions from both non-FM and FM phases, which is $J = \sum_\nu J_\nu$, with $\nu = e^\downarrow, se^\uparrow, sde^\downarrow, h^\downarrow, sh^\uparrow, sdh^\downarrow$. Here, se^\uparrow and sh^\uparrow are the spin-assisted electron and hole, respectively below T_C , influenced by the T -dependent magnetization

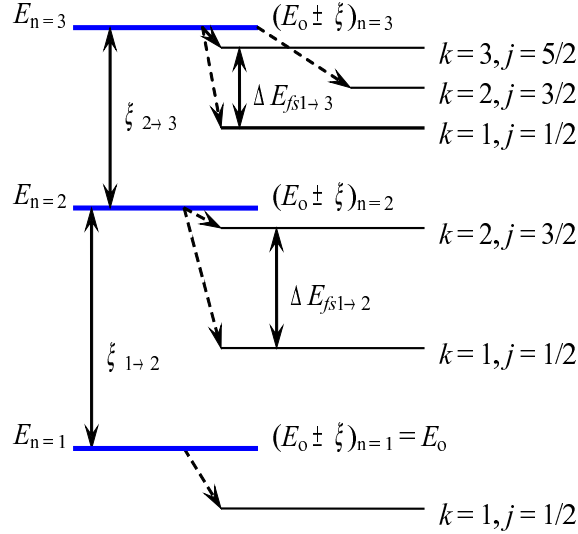


FIG. 1: Energy levels of hydrogen-like atom and the energy level splitting (not to scale). $E_{n=1,2,3}$ is the standard energy level notation while, $(E_0 \pm \xi)_{n=1,2,3}$ is the new notation introduced from Eq. (5).

function ($M(T, M_0)$) through the spin disorder scattering rate (τ_{SD}). e^\downarrow and h^\downarrow are the electron and hole with electron-electron scattering rate (τ_{e-e}). sde^\downarrow and sdh^\downarrow are the electron and hole with spin disorder scattering and $M(T, M_0) = \text{constant (Const.)}$ for $T > T_C$. For convenience, the spin-up, \uparrow denotes the direction of the magnetic field or a particular direction below T_C , while the spin-down, \downarrow represents any other direction. That is, a non-FM phase gives rise to $J_{e,h}$ and $J_{sde, sdh}$. Whereas, $J_{se, sh}$ originates from a FM phase where $(J_{sde, sdh}, J_{e,h}) \rightarrow J_{se, sh}$ for $T < T_C$. Hence, this resistivity model is fundamentally different from the phase separation model [11]. That is, $J_{e,h}(\propto \tau_{e-e}) < J_{se, sh}(\propto \tau_{SD}[M(T, M_0)])$ for $T < T_C$, while $J_{e,h}(\propto \tau_{e-e})$ and $J_{sde, sdh}(\propto \tau_{SD}[\text{Const.}])$ contribute for $T > T_C$ due to the *non-existence* of the FM phase. In other words, for $T > T_C$, the whole system is a non-FM phase and its conductivity is determined by $J_{e,h}(\propto \tau_{e-e})$ and $J_{sde, sdh}(\propto \tau_{SD}[\text{Const.}])$. For $T < T_C$, some of the non-FM phase becomes FM due to spin and its conductivity is determined by $J_{e,h} \propto \tau_{e-e}$ and $J_{se, sh}(\propto \tau_{SD}[M(T, M_0)])$. Simply put, we assume that τ_{e-e} and $\tau_{SD}[\text{Const.}]$ contribute in the non-FM phase above T_C . Below T_C , we have both FM and non-FM phases contributing to the resistivity via τ_{e-e} and $\tau_{SD}[M(T, M_0)]$. As such, the total current can be simplified as $J = J_e^\downarrow + [J_{se}^\downarrow, J_{sde}^\downarrow] = J_e + [J_{se}, J_{sde}]$ if the considered system is *n*-type, while $J = J_h + [J_{sh}, J_{sdh}]$ if it is *p*-type. J_e and J_h are the spin independent charge current due to electron and hole, respectively, and are influenced by τ_{e-e} . J_{sde} and J_{sdh} are also the spin independent charge current due to electron and hole, respectively, but are influenced by $\tau_{SD}[\text{Const.}]$ in the non-FM phase, which is valid only above T_C . J_{se} and J_{sh} are the spin-assisted charge current in the FM phase only, influenced by the $\tau_{SD}[M(T, M_0)]$. Thus, the total resistivity (for *n* or *p*-type) can be written as (after making use of the elementary resistivity equation, $\rho = m/ne^2\tau$)

$$\begin{aligned} \rho^{-1} &= \rho_{e,h}^{-1} + [\rho_{sde, sdh}^{-1}, \rho_{se, sh}^{-1}] = \left[\frac{m_{e,h}^*}{(n,p)e^2\tau_{e-e}} \right]^{-1} \\ &+ \left[\frac{m_{e,h}^*}{(n,p)e^2\tau_{SD}[\text{Const.}, M(T, M_0)]} \right]^{-1} \\ &= \left[\frac{m_{e,h}^*}{(n,p)e^2\tau_{e-e}} \right]^{-1} + \left[\frac{m_{e,h}^*}{(n,p)e^2\tau_{SD}} \right]^{-1}, \end{aligned} \quad (7)$$

where $m_{e,h}^*$ denotes the effective mass of the electron or hole. e is the charge of an electron. The carrier density for the electron and hole (n, p) based on *iFDS* (Eq. (3)) are given by (using Eq. (4))

$$n = 2 \left[\frac{k_B T}{2\pi\hbar^2} \right]^{3/2} (m_e^*)^{3/2} \exp \left[\frac{E_F - E_I}{k_B T} \right], \quad (8)$$

$$p = 2 \left[\frac{k_B T}{2\pi\hbar^2} \right]^{3/2} (m_h^*)^{3/2} \exp \left[\frac{-E_F - E_I}{k_B T} \right]. \quad (9)$$

The spin disorder scattering resistivity as derived by Tinbergen-Dekker is given by [21]

$$\begin{aligned} \rho_{SD}(T < T_C) &= \frac{(m_{e,h}^*)^{5/2} N(2E_F)^{1/2}}{\pi(n,p)e^2\hbar^4} J_{ex}^2 \\ &\times \left[S(S+1) - S^2 \left(\frac{M_{TD}(T)}{M_0} \right)^2 - S \left(\frac{M_{TD}(T)}{M_0} \right) \right. \\ &\left. \times \tanh \left(\frac{3T_C M_{TD}(T)}{2TS(S+1)M_0} \right) \right], \end{aligned} \quad (10)$$

where $M_{TD}(T, M_0)$ is the Tinbergen-Dekker magnetization function [21]. M_0 is the magnetization at zero temperature. N is the concentration of nearest neighbor ions (for example, the concentration of Mn). $\hbar = h/2\pi$, h denotes Planck's constant and S is the spin quantum number. Equation (10) is equal to the theory developed by Kasuya [22] if one replaces the term, $\tanh [3T_C M_{TD}(T)/2TS(S+1)M_0]$ with 1. Substituting $1/\tau_{e-e} = A_{e,h}T^2$ (due to the electron-electron interaction and $A_{e,h}$ is the T independent electron-electron scattering rate constant), together with Eqs. (10) and (8)(or (9)) into Eq. (7), then one can arrive at

$$\rho_{e,se}(T) = \frac{AB \exp [(E_I \mp E_F)/k_B T]}{AT^{3/2}[M_\alpha(T, M_0)]^{-1} + BT^{-1/2}}, \quad (11)$$

$$\begin{aligned} A &= \frac{A_{e,h}}{2e^2(m_{e,h}^*)^{1/2}} \left[\frac{2\pi\hbar^2}{k_B} \right]^{3/2}, \\ B &= \frac{2m_{e,h}^* N(\pi E_F)^{1/2} J_{ex}^2}{e^2\hbar k_B^{3/2}}, \\ \tau_{SD}^{-1} &= \left[\frac{N(2E_F)^{1/2}(m_{e,h}^*)^{3/2}}{\pi\hbar^4} \right] J_{ex}^2 M_\alpha(T, M_0). \end{aligned}$$

Note here that we have invoked the strong correlation through the carrier density, which is a function of the real ionization energy. Secondly, to account for different spin polarization below and above T_C , we have $n = n^\uparrow + n^\downarrow$, $1/m^* = 1/m^{*\uparrow} + 1/m^{*\downarrow}$ and $\tau = \tau_{e-e}^\downarrow + \tau_{SD}^\uparrow(J_{ex})$. Notice that the spin-disorder scattering rate, τ_{SD}^\uparrow is a function of the exchange energy, J_{ex} . Therefore, by redefining the variables in the elementary resistivity equation in accordance with strongly correlated effects, we have now derived a resistivity equation (Eq. (11)) suitable for strongly correlated ferromagnets. Here, $M_\alpha(T, M_0)$ is the T -dependent magnetization function for $T < T_C$. For $T > T_C$ however, $M_\alpha(T, M_0) = \text{constant}$. The negative and positive signs in $E_I \mp E_F$ are for electrons and holes, respectively. Equation (11) points out that, $\rho_{e,se}(T)$ is semiconducting and it only becomes metallic if $E_I \mp E_F < T$ and the FM phase sets in. Below T_C , the FM metallic phase increases with lowering T and once it achieves the maximum value (saturation) at a much lower T , insulating character may set in as a result of $E_I \mp E_F > T$. We define this temperature $T_{\text{crossover}}$ which corresponds to the transition from FM metallic to insulating below T_C . Hence, it is clear that our model is fundamentally different to the phase separation model as pointed out earlier. The emergence of insulating ($T_{\text{crossover}}$) character below T_C is an intrinsic property based on the ionization energy model, regardless of defect densities and it was first predicted for high- T_c superconductors [12]. In a recent analysis using the one- and two-orbital models, a similar insulating character below T_C was observed from numerical calculations [10], in support of our prediction. However, the analysis stops short of explaining why the insulating behavior persists even in the “clean limit” with no defects (i.e. pure host material with zero interstitial and vacancy defects). Here we propose that $T_{\text{crossover}}$ or the insulating behavior below T_C is intrinsic and is associated with the energy levels through the $E_I \mp E_F$ parameter. If $E_I \mp E_F > T > T_C$, then $\rho_{e,se}(T) \propto \exp[(E_I \mp E_F)/T]$. In this limit, a large CMR effect could be observed if the metallic-ferromagnetism sets in. The empirical function of the normalized magnetization is defined here as

$$M_\rho(T, M_0) = 1 - \frac{M_\rho(T)}{M_0}. \quad (12)$$

Equation (12) is an empirical function that will be used to extract the magnetization curve from the resistivity curve via Eq. (11). In other words, Eq. (12) is used to calculate the magnetization curve, after coupling it with Eq. (11). For example, the magnetization curves associated with Tinbergen-Dekker (TD) [21], Kasuya (K) [22] and resistivity curves (ρ) are calculated using

$$\begin{aligned} M_{TD}(T, M_0) \\ = S(S+1) - S^2 \left(\frac{M_{TD}(T)}{M_0} \right)^2 - S \left(\frac{M_{TD}(T)}{M_0} \right) \\ \times \tanh \left[\frac{3T_C M_{TD}(T)}{2TS(S+1)M_0} \right], \end{aligned} \quad (13)$$

$$\begin{aligned} M_K(T, M_0) \\ = S(S+1) - S^2 \left(\frac{M_K(T)}{M_0} \right)^2 - S \left(\frac{M_K(T)}{M_0} \right), \end{aligned} \quad (14)$$

and Eq. (12), respectively. That is, Eqs. (13), (14) and (12) are separately coupled with Eq. (11) to fit the resistivity curves and subsequently obtain $\frac{M_{TD}(T)}{M_0}$, $\frac{M_K(T)}{M_0}$ and $\frac{M_\rho(T)}{M_0}$, respectively. Consequently, we can compare and analyze $M_\alpha(T)/M_0$ with the experimentally measured, $M_{\text{exp}}(T)/M_0$ data. Recall that, $\alpha = K$ (calculated from Eq. (14)), TD (from Eq. (13)), ρ (from Eq. (12)), \exp (Experimentally determined magnetization curves). For simplicity, we will drop the term M_0 from the equations that contain $\frac{M_\alpha(T)}{M_0}$.

For the electron- or hole-doped strongly correlated non-FM semiconductors, one needs Eq. (15) given below, which is again based on *iFDS*, [12, 13, 14, 15]

$$\rho_{e,h} = AT^{1/2} \exp \left[\frac{E_I \mp E_F}{k_B T} \right], \quad (15)$$

where the $-$ sign is for the electron and $+$ sign is for the hole. Equation (15) will be used to justify the importance of the term J_{se} even if the resistivity is semiconductor-like in the FM phase.

The values of E_I can be averaged using the approximation given below

$$E_I^{\text{real}} = \beta \sum_i^z \frac{E_{Ii}}{z} \propto E_I = \sum_i^z \frac{E_{Ii}}{z}, \quad (16)$$

where β is a function of the many-body potential, $V_{\text{many-body}}$ and varies with different “background” atoms (host lattice). The $i = 1, 2, \dots, z$ represent the first, second,...etc ionization energies and, z is the oxidation number of a particular ion. E_I^{real} is actually equal to the energy needed to ionize an atom or ion in a crystal such that the electron is excited to a distance r . On the other hand, E_I corresponds to taking that particular electron to $r \rightarrow \infty$ with $V_{\text{many-body}} = 0$. Prior to averaging, the ionization energies for all the elements mentioned above were taken from Ref. 24. We can also use Eq. (17) that originates from Eq. (16) to predict the change in the valence state of a particular ion.

$$\frac{\delta}{j} \sum_{i=z+1}^{z+j} E_{Ii} + \frac{1}{z} \sum_{i=1}^z E_{Ii} = \frac{1}{q} \sum_{i=1}^q E_{Ii}. \quad (17)$$

Here, $\frac{\delta}{j} \sum_{i=z+1}^{z+j} E_{Ii}$ has $i = z+1, \dots, z+j$ and $j = 1, 2, \dots$. It is solely due to the multivalence ion. That is, the first term is due to Mn^{4+} ion’s contribution ($\text{Mn}^{3+} - \text{electron} \rightarrow \text{Mn}^{4+} = 51.200 \text{ eV atom}^{-1}$), hence j equals 1 ($= 4 - 3$) in this case and δ represents the additional contribution from Mn^{4+} . The second ($i = 1, 2, \dots, z$) and last ($i = 1, 2, \dots, q$) terms respectively are due to $\text{Mn} - 3(\text{electrons}) \rightarrow \text{Mn}^{3+}$ and $\text{Ga} - 3(\text{electrons}) \rightarrow \text{Ga}^{3+}$. Recall that $q = z = 3 +$ and $i = 1, 2, \dots$ represent the first, second,... ionization energies while $j = 1, 2, \dots$ represent the fourth, fifth,... ionization energies.

III. IONIZATION ENERGY MODEL APPLIED TO FERROMAGNETS

A. $\text{Ga}_{1-x}\text{Mn}_x\text{As}$

1. $\rho(T > T_C)$

We will first apply the E_I -based carrier density to the resistivity ($\rho(T)$) curves of DMS above T_C by means of $\rho(T > T_C) \propto 1/n$, in order to avoid the influence of fitting parameters in our analysis. Subsequently, we will discuss the evolution of resistivity curves with appropriate fittings. The $\text{Ga}_{1-x}\text{Mn}_x\text{As}$ system is the most studied material among the DMS with T_C around 170 K (Ref. 7). The origin of ferromagnetism and the transport properties in this class of materials are still unclear quantitatively [7]. The evolution of the resistivity curve ($\rho(T, x)$) for sample $X1$, $\text{Ga}_{1-x}\text{Mn}_x\text{As}$ (see Fig. 3 of Ref. 23) is such that $\rho(T, 0.015) > \rho(T, 0.022) > \rho(T, 0.035) > \rho(T, 0.043) > \rho(T, 0.053)$. That is, the $\rho(T, x)$ curve shifts downwards with increasing dopant concentration, x . This is expected from the *iFDS* model since E_I for Mn^{3+} (18.910 eV atom $^{-1}$) is less than E_I for Ga^{3+} (19.070 eV atom $^{-1}$), assuming Mn^{3+} substitutes Ga^{3+} . However, the resistivity curve, $\rho(T, 0.071)$ is above $\rho(T, 0.035)$, unexpectedly.

For sample $Y2$ (see Fig. 1 of Ref. 25), $\rho(T, 0.015) > \rho(T, 0.022) > \rho(T, 0.035)$, also complies with the *iFDS* model. Again, unexpectedly we have, $\rho(T, 0.043) < \rho(T, 0.053) < \rho(T, 0.071)$, where $\rho(T, x)$ shifts upwards with increasing x . That is, $\rho(T, x)$ switched over from decreasing (expected) to increasing with x at critical concentrations, $x_{c1} = 0.071$ and $x_{c2} = 0.043$ for samples $X1$ and $Y2$, respectively. These switch-overs that seem to violate *iFDS* can be explained if we can understand what causes E_I to deviate from its averaged value. The only reason that could give rise to such deviation is the change in the ions valence states.

Using Eq. (17), we obtain: $[\delta E_I(\text{Mn}^{4+})] + \frac{1}{3}[E_I(\text{Mn}^{3+}) + E_I(\text{Mn}^{2+}) + E_I(\text{Mn}^{1+})] = \frac{1}{3}[E_I(\text{Ga}^{3+}) + E_I(\text{Ga}^{2+}) + E_I(\text{Ga}^{1+})]$ and $(51.200 \times \delta) + 18.910 = 19.070$, therefore $\delta = 0.003$. Since the average E_I (18.910 eV atom $^{-1}$) for Mn^{3+} is less than the average E_I (19.070 eV atom $^{-1}$) for Ga^{3+} , and if the resistivity curve shifts upward with Mn substitution, then $z + \delta$ gives the minimum valence number for Mn ($\text{Mn}^{>(z+\delta)+}$) which can be calculated from Eq. (17). If however, the resistivity curve shifts downward with Mn substitution, then $z + \delta$ gives the maximum valence number for Mn ($\text{Mn}^{<(z+\delta)+}$). Consequently, the maximum valence state for Mn in $\text{Ga}_{1-x}\text{Mn}_x\text{As}$ is $3.003 + (\text{Mn}^{<3.003+})$ for the case where the $\rho(T, x)$ curve shifted downwards with x . If the valence state of Mn is larger than $3.003+$, then $\rho(T, x)$ is expected to shift upwards with x . Therefore, the switch-over from decreasing to increasing $\rho(T, x)$ with doping, x is due to larger average Mn valence state, and it is calculated to be larger than $3.003+$. Next, we need to understand what can cause this change in the average Mn valence state. The most likely reason comes from Mn occupation at non-substitutional sites, i.e., the Mn^{3+} ions do not substitute Ga^{3+} ions. This has been predicted experimentally where the formation of Mn interstitials (Mn_I) is found to be substantial above a critical concentration, x_c (Ref. 4). Interestingly, occupations at interstitial sites is found to change the charge states of Mn ions, as predicted from the first-principles calculations, where Mn^{5+} and Mn^{4+} are more stable at interstitial sites, while $\text{Mn}^{3+,2+,1+}$ are stable at substitutional sites [26]. In addition, interstitial in the presence of clustering gives rise to larger positive charge states as compared to clustering due to substitutional alone in which, larger positive charge implies larger valence state for Mn ions [26]. Therefore, we can understand that at certain doping, the average Mn valence states increased due to Mn_I and clustering and eventually reduces the carrier density and shifts the $\rho(T, x)$ curve upwards with doping.

2. $\rho(T > 0)$

Now we will apply the ionization energy incorporated resistivity model to the resistivity measurements [4] and the fits based on Eqs. (11) and (15) are shown in Figs. 2(a) and 2(b) respectively for $\text{Ga}_{1-x}\text{Mn}_x\text{As}$. One needs two fitting parameters (A and $E_I \mp E_F$) for $\rho(T > T_C)$ and another two (B and $M_\rho(T, M_0)$) for $\rho(T < T_C)$. All the fitting parameters are listed in Table I.

Note that $S = 1$ and $5/2$ are used for the fits of $M_K(T)$ while T_C and $T_{\text{crossover}}$ (T_{cr}) are determined from the experimental resistivity curves. The T_{cr} 's observed in $\text{Ga}_{0.940}\text{Mn}_{0.060}\text{As}$ (annealed: 370°C) and $\text{Ga}_{0.930}\text{Mn}_{0.070}\text{As}$ (as grown) are 10 K and 12 K, respectively, which are very close to the calculated values of 8 K and 12 K, respectively from Eq. (11). The calculated carrier density is 2×10^{20} cm $^{-3}$, using $E_I \mp E_F \sim 10$ K, and Eq. (8). In this calculation, we take the effective mass as $m_e^* = 10m_0$, in accordance with the optical spectroscopy measurements [18] and compensation due to annealing, where m_0 is the rest mass of an electron.

Figures 2(c) and 2(d) show the normalized magnetization, $M_\alpha(T)$. $M_{\rho,TD,K}(T)$ are compared with the experimentally determined magnetization [4] ($M_{\text{exp}}(T)$) as depicted in Fig. 2(d). One can easily notice the inequality, $M_{TD}(T) > M_K(T) > M_\rho(T) > M_{\text{exp}}(T)$ from Figs. 2(c) and 2(d). As such, $M_\rho(T)$ is the best fit as compared with $M_{\text{exp}}(T)$,

TABLE I: Calculated values of A , B and the ionization energy (E_I). “Ann. T ” denotes the annealing temperature and $T_{cr} = T_{crossover}$, is the temperature that corresponds to the transition from FM metallic to insulating character. “Calc.” denotes calculated values from the fits.

Samples	Ann. T (H) °C (Tesla)	A (Calc.)	B (Calc.)	$E_I \mp E_F$ (Calc.) Kelvin (meV)	T_C (T_{cr}) Kelvin
$\text{Ga}_{0.940}\text{Mn}_{0.060}\text{As}^{(a)}$	370 (0)	4.5	400	8 (0.69)	50 (10)
$\text{Ga}_{0.930}\text{Mn}_{0.070}\text{As}^{(a)}$ As grown (0)	9.2	400	-	12 (1.04)	45 (12)
$\text{Ga}_{0.930}\text{Mn}_{0.070}\text{As}^{(a)}$	370 (0)	0.02	-	280 (24.2)	-
$\text{Ga}_{0.930}\text{Mn}_{0.070}\text{As}^{(a)}$	390 (0)	0.03	-	400 (34.5)	-
$\text{La}_{0.9}\text{Ca}_{0.1}\text{MnO}_3^{(b)}$	- (0)	10	0.65	1400 (121)	222 (-)
$\text{La}_{0.8}\text{Ca}_{0.2}\text{MnO}_3^{(b)}$	- (0)	10	1.2	1300 (112)	246 (-)
$\text{La}_{0.8}\text{Ca}_{0.2}\text{MnO}_3^{(b)}$	- (6)	5	3.2	900 (78)	251 (-)

(a) Ref. [4]

(b) Ref. [28]

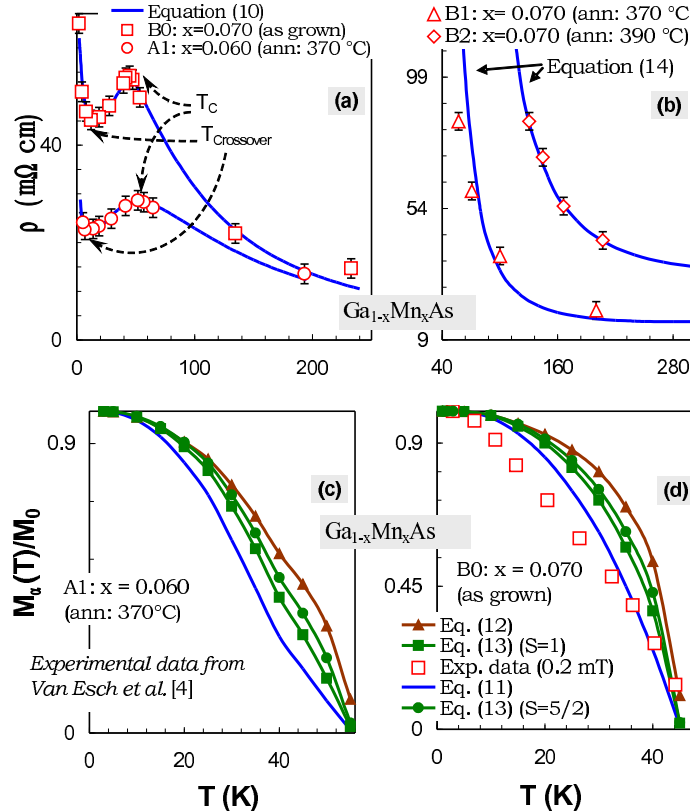


FIG. 2: (a) Calculated, using Eq. (11), and experimental resistivity curves ($\rho(T)$) as a function of temperature for $\text{Ga}_{1-x}\text{Mn}_x\text{As}$. B0 and A1 indicate $\text{Ga}_{0.930}\text{Mn}_{0.070}\text{As}$ (as grown) and $\text{Ga}_{0.940}\text{Mn}_{0.060}\text{As}$ (annealed at 370 °C), respectively. (b) Calculated, using Eq. (15), and experimental $\rho(T)$ curves for annealed non-ferromagnetic $\text{Ga}_{0.930}\text{Mn}_{0.070}\text{As}$ samples. B1 and B2 indicate $\text{Ga}_{0.930}\text{Mn}_{0.070}\text{As}$ (annealed at 370 °C) and $\text{Ga}_{0.930}\text{Mn}_{0.070}\text{As}$ (annealed at 390 °C), respectively. (c) and (d) show the T variation of calculated normalized magnetization $M_\alpha(T)$ where $\alpha = K$ (Eq. (14)), TD (Eq. (13)), ρ (Eq. (12)), exp (experimentally determined magnetization data) curves with spin quantum number $S = 1$ for $x = 0.060$ and 0.070 respectively. $M_K(T)$ is also calculated with $S = 5/2$ as shown in (c) and (d). The experimental results $M_{\text{exp}}(T)$ for $x = 0.070$ (as grown) are shown in (d).

better than the models developed by Tinbergen-Dekker [21] and Kasuya [22].

B. $\text{Mn}_x\text{Ge}_{1-x}$

1. $\rho(T > T_C)$

Another DMS material that we will consider here is the $\text{Mn}_x\text{Ge}_{1-x}$ system. It is a *p*-type DMS, with carrier density of the order of $10^{19} - 10^{20} \text{ cm}^{-3}$ for $0.006 \leq x \leq 0.035$ at room temperature [27]. From the E_I model, Mn^{3+} (18.910 eV atom $^{-1}$) substitution into Ge^{4+} (25.941 eV atom $^{-1}$) sites will shift the $\rho(T)$ curve downwards since $(E_I)_{\text{Ge}^{4+}} > (E_I)_{\text{Mn}^{3+}}$. This has been observed experimentally (see Fig. 2B of Ref. 27) where, $\rho(T, x = 0.009) > \rho(T, x = 0.016) > \rho(T, x = 0.02)$. Subsequently, we can estimate the maximum valence state for the Mn ion in $\text{Mn}_x\text{Ge}_{1-x}$ using Eq. (17) and we find, $\delta = 0.137$ or $\text{Mn}^{<3.137+}$: $[\delta E_I(\text{Mn}^{4+})] + \frac{1}{3}[E_I(\text{Mn}^{3+}) + E_I(\text{Mn}^{2+}) + E_I(\text{Mn}^{1+})] = \frac{1}{4}[E_I(\text{Ge}^{4+}) + E_I(\text{Ge}^{3+}) + E_I(\text{Ge}^{2+}) + E_I(\text{Ge}^{1+})]$. Therefore, $(51.200 \times \delta) + 18.910 = 25.941$ and $\delta = 0.137$. If the valence state of Mn is larger than 3.137+, then the $\rho(T, x)$ curve is expected to shift upwards with x . The result, $\rho(T, x = 0.02) \approx \rho(T, x = 0.033)$ indicates that Mn^{3+} in this doping range may not have substituted Ge, instead it could have occupied non-substitutional sites that eventually causes the change in the valence state of Mn. Since the resistivity, $\rho(T, x = 0.02) \approx \rho(T, x = 0.033)$, we can calculate the maximum increment of Mn^{4+} content from $x = 0.02$ to $x = 0.033$. Using $\delta = 0.137$, we estimate that there are 13.7% more Mn^{4+} in $\text{Mn}_{0.033}\text{Ge}_{0.966}$ as compared to $\text{Mn}_{0.02}\text{Ge}_{0.98}$ samples.

2. $\rho(T > 0)$

Resistivity measurements [27] and the fit using Eq. (11) are shown in Fig. 3(a). From the fit, we find that $E_I \mp E_F = 15 \text{ K}$ for $\text{Mn}_{0.02}\text{Ge}_{0.98}$ and the hole density is $2.38 \times 10^{19} \text{ cm}^{-3}$ using Eq. (8), where we take $m_h^* = m_0$, as the lower limit. This lower limit value is still comparable with the experimental value given above. We also find that the semiconductor-like behavior of $\rho(T, x = 0.02)$ below T_C is not exponentially driven as indicated by Eq. (11) in Fig. 3(a).

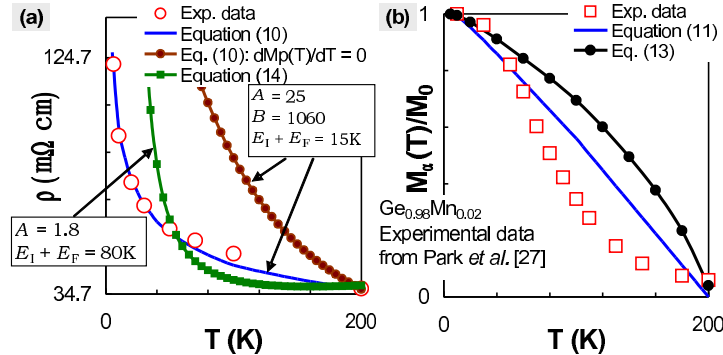


FIG. 3: (a) Calculated, using Eq. (11), and experimental resistivity curve $\rho(T)$, for $\text{Mn}_{0.02}\text{Ge}_{0.98}$. Also shown is the calculated $\rho(T)$ curve with the additional constraint, $dM_\rho(T)/dT = 0$ in Eq. (11) to emphasize the influence of $M_\rho(T)$ for an accurate fit. For these calculation, $A = 25$, $B = 1060$ and $E_I + E_F = 15 \text{ K}$. We also show that the T -dependence of $\rho(T)$ as calculated using Eq. (15) is in accordance with charge current (J_e) only. This result lacks the ability to capture the experimental result. In this case, we used $A = 1.8$ and $E_I + E_F = 15 \text{ K}$. Both $E_I + E_F = 15 \text{ K}$ and $E_I + E_F = 80 \text{ K}$ give ρ of the order of 10^{19} cm^{-3} using Eq. (8) and $m_h^* = m_0$ (rest mass). (b) shows the calculated and experimental T dependence of the magnetization curves $M_\alpha(T)$ where $\alpha = K$ (Eq. (14)), ρ (Eq. (12)), exp (experimentally determined magnetization data). Notice the inequality, $M_\rho(T) > M_{\text{exp}}(T)$ that arises as a result of the principle of least action.

The pronounced effect of Eq. (12) can be noticed by comparing the calculated plots between Eq. (11), and Eq. (11) with the additional constraint $dM_\rho(T)/dT = 0$, as depicted in Fig. 3(a). The normalized magnetization, $M_{K,\rho,\text{exp}}(T)$ for $\text{Mn}_{0.02}\text{Ge}_{0.98}$ is given in Fig. 3(b). Again, we find that $M_\rho(T)$ gives the best fit for the experimental data, which is better than $M_K(T)$ and $M_{TD}(T)$. However, $M_\rho(T)$ is significantly larger than $M_{\text{exp}}(T)$, which makes the fit poor. The reason is that the resistivity measures only the lowest E_I path, regardless of the temperature and with easily-aligned spin path that gives rise to high conductivity and complies with the principle of least action. That is, the ability of both J_e and J_{se} to follow the easiest path. On the contrary, magnetization measurements quantify the average spin of an ensemble of electrons, which will be smaller in magnitude as compared with transport measurements.

C. $\text{La}_{1-x}\text{Ca}_x\text{MnO}_3$

1. $\rho(T > T_C)$

For manganites, the $\text{La}_{1-x}\text{Ca}_x\text{MnO}_3$ system has a maximum T_C of 260 K (Ref. 28). Unlike DMS, the resistivity of this class of materials above T_C is exponential and thus gives rise to the large drop in resistance below T_C that leads to the CMR effect. We will evaluate this scenario with the ionization energy concept and show the validity of *i*FDS in both DMS and manganites. Based on E_I model, Ca^{2+} ($E_I = 9.000 \text{ eV atom}^{-1}$) < La^{3+} ($E_I = 11.940 \text{ eV atom}^{-1}$), therefore the resistivity $\rho(T, x)$ curve is expected to shift downward with Ca^{2+} doping. On the contrary, the overall $\rho(T)$ curve between $x = 0.1$ and 0.2 , above T_C are almost identical (see Fig. 3 of Ref. 28). Again, this could be due to the change in the valence state of Mn, as a result of Mn, Ca and/or La occupying the non-substitutional sites, provided that the valence states of Ca^{2+} and La^{3+} are invariant to doping and defects. Indeed, the content of Mn^{4+} is found to increase with Ca doping [28], from 19% (for $x = 0.1$) to 25% (for $x = 0.2$). We can calculate the maximum increment of Mn^{4+} from $x = 0.1$ to 0.2 , and we obtain, 5.75% using Eq. (17): $[\delta \times E_I(\text{Mn}^{4+})] + \frac{1}{2}[E_I(\text{Ca}^{2+}) + E_I(\text{Ca}^{1+})] = \frac{1}{3}[E_I(\text{La}^{3+}) + E_I(\text{La}^{2+}) + E_I(\text{La}^{1+})]$. Therefore, $(51.200 \times \delta) + 9.000 = 11.940$ and $\delta = 0.0575$. This value is remarkably close to the experimental value of 6% (=25%–19%), determined via redox titrations [28]. This implies that, $E_I^{\text{real}} \propto E_I$, which in turn implies that the averaged many-body or lattice potential (β) can be approximated as a constant. This comes as no surprise because the averaged crystal or lattice potential is indeed a constant due to the periodicity.

2. $\rho(T > 0)$

Using Eq. (11) for $\text{La}_{1-x}\text{Ca}_x\text{MnO}_3$ [28], $E_I \mp E_F$ is calculated for $x = 0.1$ and 0.2 samples and we obtain 0.121 eV (1400 K) and 0.112 eV (1300 K) respectively. The calculated carrier density, using $m^* = m_0$ and Eq. (8) gives 10^{17} cm^{-3} . In the presence of the magnetic field, $\mathbf{H} = 6 \text{ Tesla}$, we obtain $E_I \mp E_F = 0.0776 \text{ eV}$ for $x = 0.2$ and its hole concentration $p = 10^{18} \text{ cm}^{-3}$. The fits are shown in Figs. 4(a) and 4(b), while the fitting parameters are listed in Table I. The δ value determined previously (5.75 %) needs to be corrected because in the previous calculation, we used $(E_I \mp E_F)_{x=0.1} \approx (E_I \mp E_F)_{x=0.2}$ that gives maximum δ . Therefore, the actual increment after the fitting is $\delta = 5.75 \times (0.112 \text{ eV} / 0.121 \text{ eV}) = 5.32\%$.

Figures 4(c) and 4(d) depict the calculated $M_\alpha(T)$ with $S = 1$ and $M_{\text{exp}}(T)$ for $x = 0.2$, respectively. It can be seen that the magnetization curve calculated from Eq. (12) shows better agreement with the experimental data than $M_K(T)$. Hence, the ionization energy model is suitable for both types of ferromagnets, be it diluted or concentrated. However, this does not imply that the ferromagnetic interactions are identical between diluted and concentrated ferromagnets.

IV. CONCLUSIONS

In conclusion, we have developed a theoretical model based on the ionization energy concept that can be used to analyze the evolution of the resistivity versus temperature curves of both diluted and concentrated ferromagnets, for different doping elements. By identifying the cause that deviate the ionization energy from its averaged value, we come to understand how defects and clustering contribute to the changes in valence states of ions and eventually how they affect the resistivity of ferromagnets.

Acknowledgments

ADA is grateful to the University of Sydney for the USIRS award. Special thanks to A. Stroppa for his explanation on the half-metallic character of MnGe and MnSi. X. Y. Cui and C. Stampfl gratefully acknowledge support from the Australian Research Council (ARC). KR acknowledges partial funding from the Malaysian grant No. SAGA 66-02-03-0077.

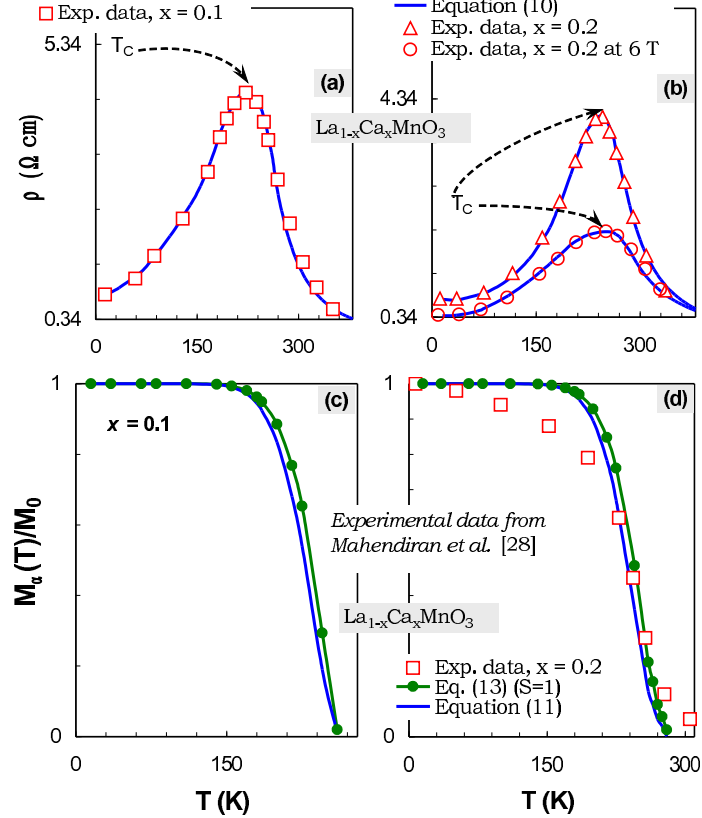


FIG. 4: (a) shows the experimental results for the resistivity versus temperature, $\rho(T)$, for $\text{La}_{1-x}\text{Ca}_x\text{MnO}_3$ for $x = 0.1, 0.2$ and 0.2 (6 Tesla) and (b) the calculated $\rho(T)$ using Eq. (11). All fits are indicated with solid lines. (c) and (d) show the T variation of the magnetization, $M_\alpha(T)$, where $\alpha = K$ (Eq. (14)) and ρ (Eq. (12)) with $S = 1$ for $x = 0.1$ and 0.2 , respectively. The experimental $M_{\text{exp}}(T)$ curve for $x = 0.2$ is given in (d).

V. APPENDIX

A. 1D harmonic oscillator: ionization energy as the eigenvalue

The one-dimensional Hamiltonian of mass m moving in the presence of potential, $V(x)$ is given by (after making use of the linear momentum operator, $\hat{p} = -i\hbar\partial^2/\partial x^2$) [29],

$$\left[-\frac{\hbar^2}{2m} \frac{\partial^2}{\partial x^2} + V(x) \right] \varphi = E\varphi, \\ = (E_{\text{kin}} + V_{\text{pot}})\varphi, \quad (18)$$

where E , E_{kin} , $V(x)$ and V_{pot} denote the total energy, kinetic energy, potential energy operator and the potential energy, respectively.

We define,

$$\pm \xi := E_{\text{kin}} - E_0 + V_{\text{pot}}, \quad (19)$$

such that $\pm \xi$ is the energy needed for a particle to overcome the bound state and the potential that surrounds it. The + sign for $\pm \xi$ is for the electron ($0 \rightarrow +\infty$) while the - sign is for the hole ($-\infty \rightarrow 0$). E_{kin} and E_0 denote the total energy at $V_{\text{pot}} = 0$ and the energy at $T = 0$, respectively, i.e., $E_{\text{kin}} = \text{kinetic energy}$. In physical terms, ξ is defined as the ionization energy. That is, ξ is the energy needed to excite a particular electron to a finite distance, r , not necessarily $r \rightarrow \infty$.

On the other hand, using the above stated new definition (Eq. (19)) and the condition, $T = 0$ and $V_{\text{pot}} = 0$, we can rewrite the total energy as

$$E = E_{\text{kin}} = E_0 \pm \xi. \quad (20)$$

From Eq. (19) we have $E = E_0 \pm \xi = E_{\text{kin}} + V_{\text{pot}}$, therefore

$$\hat{H}\varphi = (E_0 \pm \xi)\varphi, \quad (21)$$

where the total energy is given by $E = E_0 \pm \xi$ and φ is the ionization energy based wavefunction while \hat{H} is the Hamilton operator.

Proof: Assume a solution for Eq. (21) at $n = 0$ state (ground state) in the form of $\varphi_{n=0}(x) = C \exp[-ax^2]$ in order to be compared with the standard harmonic oscillator wavefunction [29],

$$\varphi_0(x) = \left[\frac{m\omega}{\pi\hbar} \right]^{1/4} \exp \left[-\frac{m\omega}{2\hbar} x^2 \right], \quad (22)$$

where $\hbar = h/2\pi$, h is Planck's constant and ω is the frequency. Therefore, we obtain $\ln \varphi(x) = \ln C - ax^2 \ln e$, $\frac{1}{\varphi(x)} \frac{\partial \varphi(x)}{\partial x} = -2ax$ and $\frac{\partial^2 \varphi(x)}{\partial x^2} = 2a\varphi(x)[2ax^2 - 1]$. On the other hand, we can rewrite Eq. (21) to obtain

$$\frac{\partial^2 \varphi}{\partial x^2} = -\frac{2m}{\hbar^2} [E_0 \pm \xi] \varphi, \quad (23)$$

where E and E_0 for a given system range from $+\infty$ to 0 for electrons and 0 to $-\infty$ for holes which explains the \pm sign in ξ . Using Eqs. (18), (21) and, (23), we obtain $a = \frac{m}{\hbar^2}(E_0 \pm \xi)$. Normalizing φ gives

$$\begin{aligned} 1 &= \int_{-\infty}^{+\infty} |\varphi(x)|^2 dx = 2|C|^2 \int_0^{+\infty} e^{-2ax^2} dx \\ &= 2|C|^2 \frac{1}{2} \left[\frac{\pi}{2a} \right]^{1/2} \end{aligned} \quad (24)$$

and $C = \left[\frac{2m(E_0 \pm \xi)}{\pi\hbar^2} \right]^{1/4}$. Consequently,

$$\varphi(x) = \left[\frac{2m(E_0 \pm \xi)}{\pi\hbar^2} \right]^{1/4} \exp \left[-\frac{m}{\hbar^2}(E_0 \pm \xi)x^2 \right]. \quad (25)$$

Now, we compare Eq. (25) with Eq. (22). In doing so, we can show that the ground state energy is,

$$\frac{1}{2}\hbar\omega = E_0 \pm \xi, \quad (26)$$

either from equating $[m\omega/\pi\hbar]^{1/4} = [2m(E_0 \pm \xi)/\pi\hbar^2]^{1/4}$ or $-mx^2\omega/2\hbar = -m(E_0 \pm \xi)x^2/\hbar^2$.

B. Expectation value for $\mathbf{V}(\mathbf{x})$

In this section, we will show that the total energy, $E_0 \pm \xi$ is a function of the potential energy. That is, using Eqs. (18), (19) and (21), we will show the potential energy can be written in terms of $E_0 \pm \xi$. For example, from Eq. (25) the harmonic oscillator Schrodinger Eq. can be shown as

$$-\frac{\hbar^2}{2m} \frac{\partial^2 \varphi}{\partial x^2} = \left[\frac{2m}{\hbar^2} (E_0 \pm \xi)^2 x^2 - (E_0 \pm \xi) \right] \varphi. \quad (27)$$

Therefore, the potential energy is given by

$$V(x) = \frac{2m}{\hbar^2} (E_0 \pm \xi)^2 x^2. \quad (28)$$

Proof: From Eq. (28), we can write

$$\hat{H} = \frac{1}{2m} \left[\hat{p}^2 + \left(\frac{2m}{\hbar} (E_0 \pm \xi) x \right)^2 \right]. \quad (29)$$

Therefore, the ladder operator can be written as

$$a_{\pm} = A \left[\mp i\hat{p} + \left(\frac{2m}{\hbar} (E_0 \pm \xi) \right) x \right]. \quad (30)$$

A is a factor that will be used to derive the expectation value of $V(x)$. Taking $K = \frac{2m}{\hbar} (E_0 \pm \xi)$, we obtain

$$a_{\pm} = A [\mp i\hat{p} + Kx]. \quad (31)$$

Since the commutation relation [29], $[x, \hat{p}] = i\hbar$, then

$$[a_-, a_+] = 2A^2 K \hbar = -[a_+, a_-]. \quad (32)$$

Using Eq. (29), we get

$$a_- a_+ = A^2 (2m\hat{H} + K\hbar), \quad (33)$$

$$\hat{H} = \frac{1}{2m} \left[\frac{a_+ a_-}{A^2} \mp K\hbar \right]. \quad (34)$$

Consequently, we can show that

$$\begin{aligned} \hat{H}(a_+ \varphi) &= \frac{1}{2m} \left[\frac{a_+ a_-}{A^2} + K\hbar \right] (a_+ \varphi) \\ &= (E_0 \pm \xi) \varphi. \end{aligned} \quad (35)$$

Subsequently, $\hat{H}(a_- \varphi) = [E_0 \pm \xi - 2(E_0 \pm \xi)] a_- \varphi$. Applying the condition [29] for the ground state, $\varphi_{n=0}$ such that

$$a_- \varphi_{n=0} = 0, \quad (36)$$

will lead us to

$$E_{n=0} \varphi_{n=0} = \hat{H} \varphi_{n=0} = (E_0 \pm \xi) \varphi_{n=0}. \quad (37)$$

Recall that E_0 is the energy at $T = 0$ and $E_{n=0}$ denotes the energy for the $n = 0$ state. Finally, utilizing Eqs. (37) and (35), we obtain

$$E_n = (1 + 2n)(E_0 \pm \xi). \quad (38)$$

Subsequently, we find that (using Eqs. (21), (34) and (38))

$$\begin{aligned} a_+ a_- \varphi_n &= n2A^2 K \hbar \varphi_n, \\ a_- a_+ \varphi_n &= (n + 2A^2 K \hbar) \varphi_n \Leftrightarrow [a_-, a_+] = 2A^2 K \hbar. \end{aligned}$$

Now, using the identity [29]

$$\int_{-\infty}^{\infty} (f^*)(a_{\pm}g)dx = \int_{-\infty}^{\infty} (a_{\mp}f^*)(g)dx,$$

We find

$$\begin{aligned} \int_{-\infty}^{\infty} (a_{+}\varphi_n)^*(a_{+}\varphi_n)dx &= \int_{-\infty}^{\infty} (a_{-}a_{+}\varphi_n)^*\varphi_n dx \\ &= (n + 2A^2K\hbar) \int_{-\infty}^{\infty} |\varphi_n|^2 dx, \\ \int_{-\infty}^{\infty} (a_{-}\varphi_n)^*(a_{-}\varphi_n)dx &= \int_{-\infty}^{\infty} (a_{+}a_{-}\varphi_n)^*\varphi_n dx \\ &= n2A^2K\hbar \int_{-\infty}^{\infty} |\varphi_n|^2 dx. \end{aligned}$$

On the other hand, we have

$$a_{\pm}\varphi_n \propto \varphi_{n\pm 1} \Rightarrow a_{\pm}\varphi_n = \gamma_n^{\pm}\varphi_{n\pm 1},$$

where γ_n^+ and γ_n^- are the proportionality factors, which can be determined from

$$\int_{-\infty}^{\infty} (a_{\pm}\varphi_n)^*(a_{\pm}\varphi_n)dx = |\gamma_n^{\pm}|^2 \int_{-\infty}^{\infty} |\varphi_{n\pm 1}|^2 dx,$$

hence, we can now write $a_{+}\varphi_n = (n + 2A^2K\hbar)^{1/2}\varphi_{n+1}$ and

$$a_{-}\varphi_n = (n2A^2K\hbar)^{1/2}\varphi_{n-1}. \quad (39)$$

We can rearrange Eq. (31) to get

$$x^2 = \frac{(a_{+} + a_{-})^2}{4A^2K^2}. \quad (40)$$

As a consequence, (from Eqs. (31) and (40), also invoking the orthogonality in the last step)

$$\begin{aligned} \langle V(x) \rangle &= \left\langle \frac{2m}{\hbar^2} (E_0 \pm \xi)^2 x^2 \right\rangle \\ &= \frac{2A^2K\hbar(1+n) + n}{8A^2m}. \end{aligned} \quad (41)$$

From Eq. (38), we know that

$$\langle V(x) \rangle = \frac{1}{2}(1+2n)(E_0 \pm \xi), \quad (42)$$

the other half is due to kinetic energy [29]. Putting Eqs. (41) and (42) together leaves us with

$$\frac{2A^2K\hbar(1+n) + n}{8A^2m} = \frac{1}{2}(1+2n)(E_0 \pm \xi), \quad (43)$$

Therefore $A^2 = \frac{1}{2K\hbar}$. Hence, the commutation relation given in Eq. (32) can be rewritten as

$$[a_-, a_+] = 2A^2K\hbar = 1 = -[a_+, a_-]. \quad (44)$$

As a result of this, indeed the potential energy is given in terms of $E_0 \pm \xi$ from Eq. (42).

[1] Zutic I, Fabian J and Das Sarma S 2004 *Rev. Mod. Phys.* **76** 323.

[2] Munekata H, Ohno H, von Molnar S, Segmuller A, Chang L L and Esaki L 1989 *Phys. Rev. Lett.* **63** 1849.

[3] von Helmolt R, Wecker J, Holzapfel B, Schultz L and Samwer K 1993 *Phys. Rev. Lett.* **71** 2331.

[4] Van Esch A, Van Bockstal L, De Boeck J, Verbanck G, van Steenbergen A S, Wellmann P J, Grietens B, Bogaerts R, Herlach F and Borghs G 1997 *Phys. Rev. B* **56** 13103.

[5] Omiya T, Matsukura F, Dietl T, Ohno Y, Sakon T, Motokawa M and Ohno H 2000 *Physica E* **7** 976.

[6] Luttinger J M and Kohn W 1955 *Phys. Rev.* **97** 869.

[7] Jungwirth T, Sinova J, Macek J, Kucera J and MacDonald A H 2006 *Rev. Mod. Phys.* **78** 809.

[8] Hwang E H and Das Sarma S 2005 *Phys. Rev. B* **72** 35210.

[9] Lopez-sancho M P and Brey L 2003 *Phys. Rev. B* **68** 113201.

[10] Sen C, Alvarez G, Aliaga H and Dagotto E 2006 *Phys. Rev. B* **73** 224441.

[11] Mayr M, Moreo A, Verges J A, Arispe J, Feiguin A and Dagotto E 2000 *Phys. Rev. Lett.* **86** 135.

[12] Arulسامي A D 2001 *Physica C* **356** 62.

[13] Arulسامي A D 2002 *Phys. Lett. A* **300** 691.

[14] Arulسامي A D 2004 in *Superconductivity research at the leading edge* (ed Lewis, P. S.) 45 (Nova Science Publishers, New York).

[15] Arulسامي A D 2005 *Phys. Lett. A* **334** 413.

[16] Anderson P W 1972 *Science* **177** 393.

[17] Arulسامي A D arXiv:physics/0702232.

[18] Burch K S, Shrekenhamer D B, Singley E J, Stephens J, Sheu B L, Kawakami R K, Schiffer P, Samarth N, Awschalom D D and Basov D N 2006 *Phys. Rev. Lett.* **97** 87208.

[19] Bethe H A and Salpeter E E 1957 *Quantum mechanics of one- and two-electron atoms* (Springer-Verlag, Berlin).

[20] Murakami S, Nagaosa N and Zhang S C 2003 *Science* **301** 1348.

[21] Tineke Van Peski-Tinbergen and Dekker A J 1963 *Physica* **29** 917.

[22] Kasuya T 1956 *Prog. Theor. Phys.* **16** 58.

[23] Matsukura F, Ohno H, Shen A and Sugawara Y 1998 *Phys. Rev. B* **57** R2037.

[24] Winter M J <<http://www.webelements.com>>.

[25] Oiwa A, Katsumoto S, Endo A, Hirasawa M, Iye Y, Ohno H, Matsukura F, Shen A and Sugawara Y 1997 *Solid State Commun.* **103** 209.

[26] Mahadevan P and Zunger A 2003 *Phys. Rev. B* **68** 75202.

[27] Park Y D, Hanbicki A T, Erwin S C, Hellberg C S, Sullivan J M, Matson J E, Ambrose T F, Wilson A, Spanos G and Jonker B T 2002 *Science* **295** 651.

[28] Mahendiran R, Tiwary S K, Raychaudhuri A K, Ramakrishnan T V, Mahesh R, Rangavittal N and Rao C N R 1996 *Phys. Rev. B* **53** 3348.

[29] Griffiths D J 1995 *Introduction to quantum mechanics* (Prentice-Hall, New Jersey).